

DOCKETED

Docket Number:	16-IEPR-04
Project Title:	Climate Adaptation and Resiliency
TN #:	211804
Document Title:	Dynamically Downscaled CMIP5 Climate Projections Over California
Description:	Alex Hall, Fengpeng Sun, Daniel B. Walton, Marla Schwartz, Neil Berg, and Katharine Reich
Filer:	Raquel Kravitz
Organization:	California Energy Commission
Submitter Role:	Commission Staff
Submission Date:	6/14/2016 10:18:24 AM
Docketed Date:	6/14/2016

Dynamically Downscaled CMIP5 Climate Projections Over California

Alex Hall, Fengpeng Sun, Daniel B. Walton, Marla Schwartz, Neil Berg, and Katharine Reich

University of California, Los Angeles
Department of Atmospheric and Oceanic Sciences
Math Sciences Building 7127
Los Angeles, CA 90095-1565

UCLA is making available to researchers participating in California's 4th Climate Change Assessment a high-resolution climate data set comprising 1) a simulation of historical climate from 1981–2014 and 2) projections of future climate from 2091–2101. The five future projections represent dynamically downscaled output from five global climate models from the Coupled Model Intercomparison Project, Phase 5 (CMIP5; Taylor et al. 2012), the latest generation of global climate model experiments used in the Intergovernmental Panel on Climate Change's 5th Assessment Report.

This document describes the UCLA dynamically downscaled data set, explains the methodology employed to create it, and provides caveats for its use.

Data set description

Available in the UCLA data set are six simulations of present and future climate:

- 1) "Baseline" simulation of historical climate, covering October 1981 through September 2014
- 2) Projection of future climate, covering October 2091 through September 2101, created with the climate change signal from CNRM-CM5 global climate model
- 3) Projection of future climate, covering October 2091 through September 2101, created with the climate change signal from GFDL-CM3 global climate model
- 4) Projection of future climate, covering October 2091 through September 2101, created with the climate change signal from Inmcm4 global climate model
- 5) Projection of future climate, covering October 2091 through September 2101, created with the climate change signal from IPSL-CM5A-LR global climate model
- 6) Projection of future climate, covering October 2091 through September 2101, created with the climate change signal from MPI-ESM-LR global climate model

All simulations were created using the Weather Research and Forecasting (WRF) model version 3.5 (Skamarock et al. 2008). For the baseline simulation, WRF was forced at the study domain's boundaries by data from the North American Regional Reanalysis (NARR; Mesinger et al. 2006). For each future projection, historical NARR data were perturbed by the climate change signal given by the global climate model in use, then used to drive the WRF model. For a more detailed description of our methods, including the rationale for the selection of global climate models used in the future projections, see the "Methodology" section below.

Greenhouse gas concentration scenario: The five future simulations correspond to the IPCC Representative Concentration Pathway 8.5 (RCP8.5). This pathway represents a "business as usual" scenario in which greenhouse gas concentrations continue to increase throughout the 21st century. For more information, a "Beginner's Guide to the Representative Concentration Pathways" is available at http://www.skepticalscience.com/docs/RCP_Guide.pdf.

Spatial resolution: 9-km resolution over California (Figure 1, "D2"); 3-km resolution over the Sierra Nevada range (Figure 1, "D3")

Temporal resolution: 30-minute resolution for surface air temperature; 6-hourly resolution for all other variables.

Available variables: All six historical and future simulations include the complete set of variables outputted by the WRF model. A partial list is provided here. For the full list, visit http://www2.mmm.ucar.edu/wrf/users/docs/user_guide_V3.5/users_guide_chap5.htm#fields

2-Dimensional Surface Variables

Temperature at 2 meters
Precipitation
Humidity
Surface pressure
Surface heat fluxes
Surface moisture flux
Surface runoff
Soil temperature
Soil moisture
Snow cover
Snow density
Snow depth
Snow water equivalent

3-Dimensional Variables

Temperature
Humidity
Zonal wind
Meridional wind
Geopotential

Context for data set creation

Because California’s Sierra Nevada is a critical source of the state’s freshwater, the UCLA team designed a downscaling study with this region as the focus. California’s Sierra Nevada is a high-elevation mountain range with complex topography and significant seasonal snow cover. Anthropogenic warming in the region is expected to cause large reductions in snowpack by the end of the 21st century (Pierce et al. 2013a). Areas experiencing snow cover loss are subject to extra warming due to snow albedo feedback. The disappearance of snow reveals lower albedo surfaces, which causes an increase in absorbed solar radiation and further warming. Snow albedo feedback is a critical feature of climate change in snow covered regions that leads to elevation dependent outcomes (Giorgi et al. 1997; Kim 2001; Rangwala and Miller 2012; Pepin et al. 2015; Letcher and Minder et al. 2015). Although snow albedo feedback is a feature of climate change present in global climate models (Qu and Hall, 2014), global climate models largely miss its effect in areas of intense topography due to their low resolution (~100–200 km). In the case of the Sierra Nevada, their resolution is generally too low to resolve this mountain complex and the structure of snow cover therein. To provide future projections that capture the effect of snow albedo feedback on the warming in the Sierra Nevada, much higher resolution is necessary.

A variety of approaches are available for downscaling global climate model output to higher resolution (Wilby and Wigley 1997; Benestad et al. 2008; Maraun et al. 2010). One approach, dynamical downscaling, explicitly simulates the complex physical processes that underlie the local climate response using a regional climate model (RCM) forced at its boundaries by global climate model output. Dynamical downscaling may be an advantageous approach to downscaling global climate models over the Sierra Nevada as it directly simulates both snow albedo feedback and the inhibition of mixing of air masses due to the high peaks. While dynamical downscaling can simulate critical mechanisms associated with regional climate change, it also introduces additional errors and uncertainty. An RCM may drift towards a climate different than its driving global climate model and may produce widely varying results depending on the choice of parameterizations and resolution. Furthermore, dynamically downscaling a large ensemble of global climate models—critical for computing ensemble-mean outcomes and

characterizing uncertainty associated with global climate model spread—is usually impractical because of its high computational cost.

A second approach, statistical downscaling, employs statistical relationships from the historical period to transform low-resolution predictors into high-resolution predictands (Benestad et al. 2008). Statistical downscaling generally has a much lower computational cost, making it a valuable tool for downscaling multi-model ensembles and producing more robust estimates of likely outcomes and uncertainty (Giorgi et al. 2001; Tebaldi et al. 2005; Pierce et al. 2013a,b). However, the empirical relationships between large and fine scales employed in statistical downscaling can break down under climate change (Gutierrez et al. 2013; Dayon et al. 2015; Dixon et al. 2016).

A third approach, hybrid dynamical-statistical downscaling (Walton et al. 2015), uses a statistical model to extend the results of dynamical downscaling to multiple global climate models. Under this approach, dynamical downscaling is applied to a small subset of global climate models. Then the output is used to build a simple statistical model to mimic the behavior of the dynamical model and downscale the results for the remaining global climate models in the ensemble. This approach adds a layer of complexity to the downscaling process, but it also provides valuable gains. It can capture important features of the warming pattern that may be present only in dynamical downscaling, but a fraction of dynamical downscaling's computational cost (Berg et al. 2015; Sun et al. 2015; Walton et al. 2015).

The dynamically downscaled projections created by UCLA form the basis of a hybrid dynamical-statistical downscaling study over the Sierra Nevada. Results from that study are described in Walton et al. 2016.

In the following sections, we describe how we perform dynamical downscaling to generate historical and future high-resolution simulations. Then, we evaluate the realism of the historical simulation by comparing to observationally based gridded datasets. Finally, we examine the climate change patterns generated by differencing the future and historical simulations.

Methodology: Dynamical downscaling with WRF

Dynamically downscaled simulations are performed using the Weather Research and Forecasting (WRF) model version 3.5 (Skamarock et al. 2008). WRF is coupled to the community Noah land surface model with multiparameterization options (Noah-MP; Niu et al. 2011). Three one-way nested domains (27, 9, and 3 km resolution, going from the outermost to innermost domain) are used (Figure 1a). In each domain, all variables within five grid cells from the horizontal lateral boundary are relaxed towards the corresponding values at the boundaries. To provide a better representation of surface and boundary layer processes, the model's vertical resolution is enhanced near the surface, with 30 out of 43 total sigma levels below 3 km. The package of physical parameterizations consists of the New Thompson microphysics scheme (Thompson et al. 2008), Dudhia shortwave radiation scheme (Dudhia 1989), Rapid Radiative Transfer Model longwave (RRTM) longwave radiation scheme (Mlawer et al. 1997), MYNN Level 2.5 surface/boundary layer scheme (Nakanishi and Niino 2006, and Old Kain-Fritsch cumulus convection scheme (Kain and Fritsch 1990). Spectral nudging of temperature, zonal and meridional winds and geopotential height above the boundary layer (roughly at 850 hPa) is employed over the outermost domain. In this study we focus only on climate information from the innermost domain, which goes from the eastern edge of the Central Valley to the leeside of the California Sierra Nevada (Figure 1b).

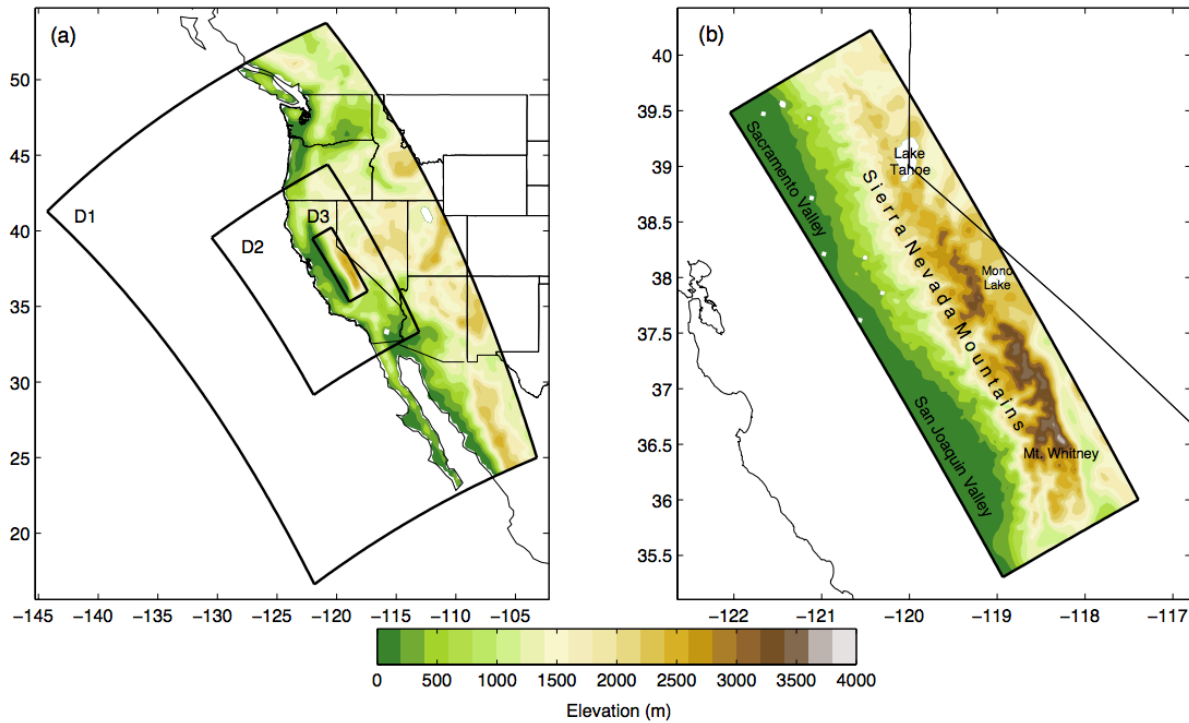


Figure 1: (a) Topography (meters) and model setup with three one-way nested WRF domains (D1, D2, and D3) at resolutions of 27, 9, and 3 km. (b) Innermost domain (D3) topography.

Climatic changes are projected using a single baseline simulation and five future simulations, following the pseudo-global warming method (Schär et al. 1996; Sato et al. 2007; Kawase et al. 2009; Rasmussen et al. 2011). The baseline simulation spans the 1981–2006¹ period and is forced at the surface and along the outermost boundary with 6-hourly North American Regional Reanalysis (NARR; Mesinger et al. 2006). The baseline simulation is used to evaluate WRF’s ability to simulate regional climate through comparison with the observational record (Section 2b). The 1991–2000 sub-period is used to compare with the future simulations. The five future simulations represent how the weather and climate of the 1991–2000 historical sub-period would have unfolded if the mean climate were altered to reflect the climate change signals found in five CMIP5 global climate models run under the RCP 8.5 scenario. The five global climate models used here (CNRM-CM5, GFDL-CM3, Inmcm4, IPSL-CM5A-LR, and MPI-ESM-LR) were selected to span the approximate range of temperature and precipitation changes over California of the full CMIP5 ensemble (Figure 2). Each future simulation is forced with boundary conditions created by adding the difference in global climate model monthly climatology (2081–2100 minus 1981–2000) to the 1991–2000 NARR data. This process was applied to temperature, humidity, zonal and meridional winds, and geopotential height. The future WRF simulations are then differenced with the 1991–2000 portion of the baseline WRF simulation to determine the regional climate change signals. Because each future year has the same climatological perturbation added to the boundary conditions, only a few downscaled future years are necessary to determine the regionalized climate change signals. Thus, a 10-year sub-period is used for future simulations to conserve scarce computational resources.

¹ Note that the time periods in this section of the document differ slightly from those specified on page 1. Time periods in this section reflect data availability at the time the methodology was developed and initial analysis was conducted. Since then, additional years have been added to our simulations.

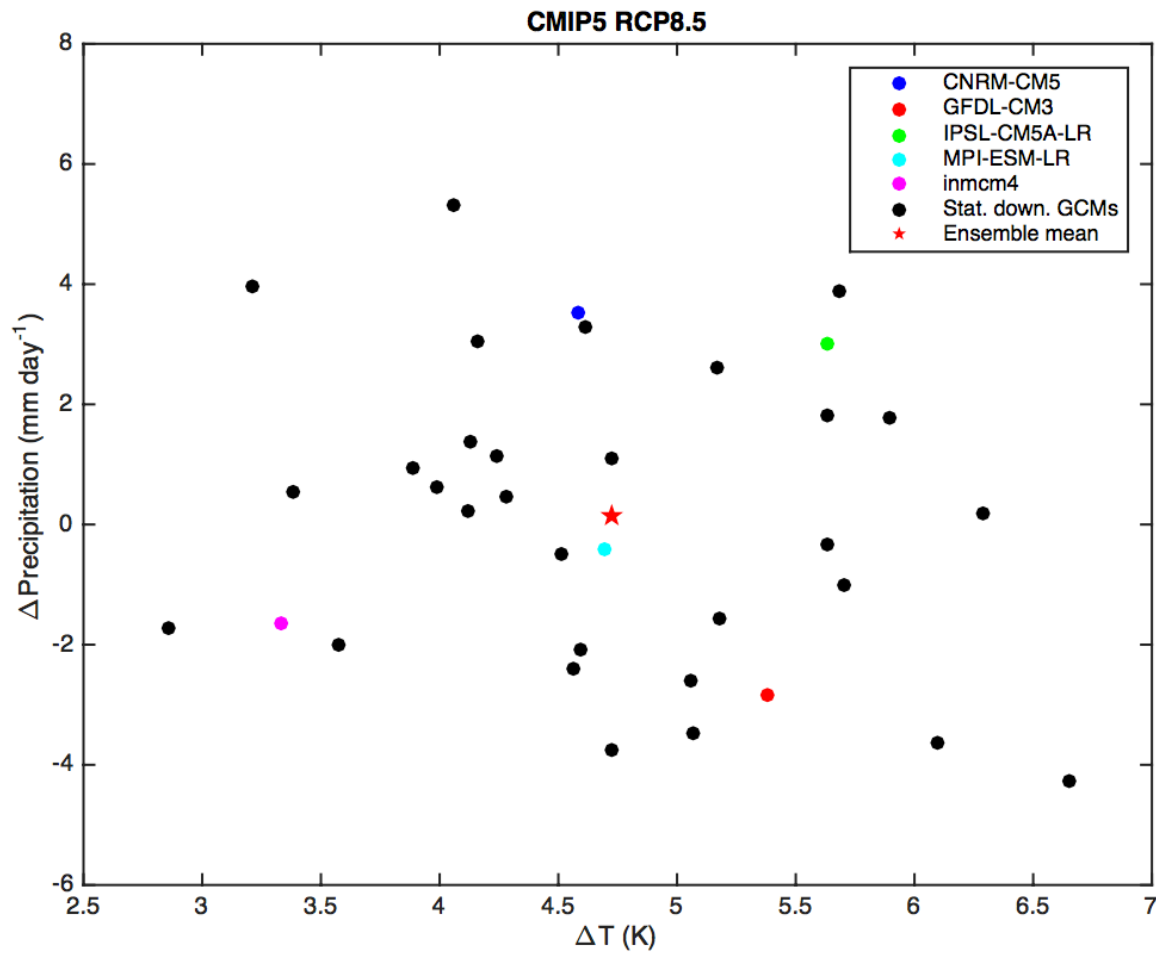


Figure 2: Changes in annual-mean precipitation (mm day^{-1}) versus annual-mean changes in surface air temperature (K) averaged over California in 35 CMIP5 global climate models (GCMs) run under the RCP8.5 scenario. The five GCMs selected for dynamical downscaling are highlighted (colors). The black dots represent GCMs that are downscaled with the hybrid statistical model. The ensemble mean (all GCMs) is indicated with a red star.

There are several noteworthy advantages and disadvantages of the pseudo-global warming method. First, forcing the baseline simulation with reanalysis allows for direct comparison of the baseline simulation to historical observations. If raw global climate model output were used as forcing instead, then only statistical properties could be compared. Furthermore, by using reanalysis for the baseline simulation (and perturbed reanalysis for the future simulations), we avoid subjecting the simulations to potentially large biases in mean state often found in global climate models. This may be particularly important in regions where snow albedo feedback plays an important role in warming. For example, significant temperature biases in the mean state would lead to unrealistic snow cover, and hence unrealistic amplification of warming due to snow albedo feedback when the climate state is perturbed. A downside to the pseudo-global warming method is that the future simulations are driven by mean climatological perturbations to the historical boundary conditions, so no changes in large-scale interannual variability are downscaled. (However, changes in the mean state may affect how variability develops inside the WRF domain.) The benefit of this approach is that the historical variability captured in the reanalysis is much more realistic than what is simulated in global climate models. For example, many global climate models struggle to realistically simulate El Niño / Southern Oscillation (Guilyardi et al. 2009), a key source of variability in California’s climate. So we would not have a high level of trust in the changes in variability predicted by global climate models, even if they were included. Still, because our methodology excludes global climate model-driven variability changes, we must limit the scope of this study to changes in mean climate.

Evaluation of the WRF baseline simulation

An evaluation of surface air temperature and snow cover output from the WRF baseline simulation is presented in Figures 3 and 4, respectively. WRF temperature output (3-km resolution) is compared to output from the Parameter-elevation Relationships on Independent Slopes Model (PRISM; Daly et al. 2008), an observationally-based gridded product at 4 km resolution. The PRISM dataset is not strictly speaking an observational data set, as it incorporates assumptions about how climate fields vary in the many areas where observations are unavailable. However, it is independently-derived from the WRF baseline simulation, and in this sense provides a check on its realism. PRISM data is stored in monthly averages of daily maximum and minimum temperatures, which we averaged to generate monthly mean temperatures. For comparison purposes, PRISM data has been linearly interpolated to 3 km resolution, matching the WRF grid. The linearly interpolated PRISM data is also adjusted to account for the difference in elevation between the interpolated PRISM grid and the WRF grid, using a lapse rate of $6.5\text{ }^{\circ}\text{C km}^{-1}$.

Differences between WRF and PRISM in climatological annual-mean temperatures for the 1981–2000 period are generally small (Figure 3a-c), averaging out over the domain to only $-0.1\text{ }^{\circ}\text{C}$. However, WRF tends to be colder ($-1.2\text{ }^{\circ}\text{C}$) at higher elevations ($> 2500\text{ m}$), especially in the northern Sierra Nevada. WRF and PRISM report similar composite seasonal cycles, which are calculated by averaging the temperature for each calendar month over the 1981–2000 period. The mean absolute error (MAE) between the twelve monthly values making up the seasonal cycle (Figure 3d) has a domain average of $1.0\text{ }^{\circ}\text{C}$, with slightly larger errors ($1.5\text{ }^{\circ}\text{C}$) at higher elevations ($> 2500\text{ m}$).

The temporal variability of surface air temperature also shows strong agreement between WRF and PRISM. A comparison of monthly-mean temperature anomalies in WRF and PRISM is shown in Figure 3e. The WRF and PRISM anomalies are highly correlated (Figure 3e), with an average correlation of 0.95 over the domain. Moreover, the mean absolute error (MAE) in monthly anomalies is also generally small, with the largest errors again found at higher elevations (Figure 3f). Taken as a whole, Figure 3 shows that WRF accurately simulates the baseline temperature climatology and temporal variability, albeit with a slight cold bias at higher elevations.

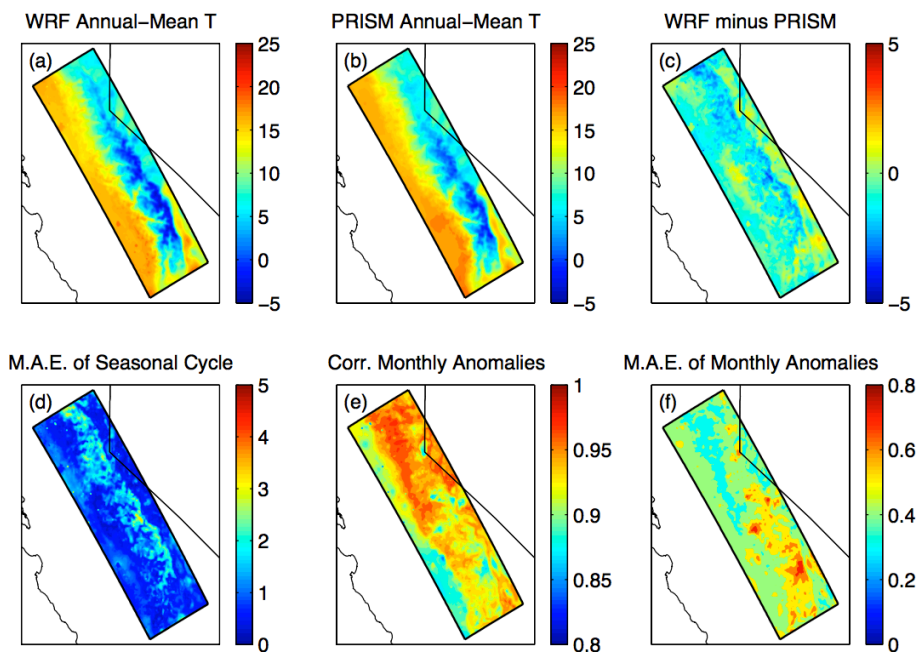


Figure 3: Comparison of WRF and PRISM temperatures (1981–2000). PRISM temperatures are interpolated to the WRF 3 km grid and adjusted based on a lapse rate of 6.5 K/km to correct for the mismatch between WRF elevations and the interpolated PRISM elevations. Shown are the annual Tavg climatologies for (a) WRF, (b) PRISM, (c) WRF minus PRISM. (d) Mean absolute error between the composite seasonal cycles (twelve monthly values of Tavg) of WRF and elevation-corrected PRISM. (e) Correlations of monthly temperature anomalies (relative to composite 1981–2001 seasonal cycle). (f) Mean absolute error of monthly temperature anomalies.

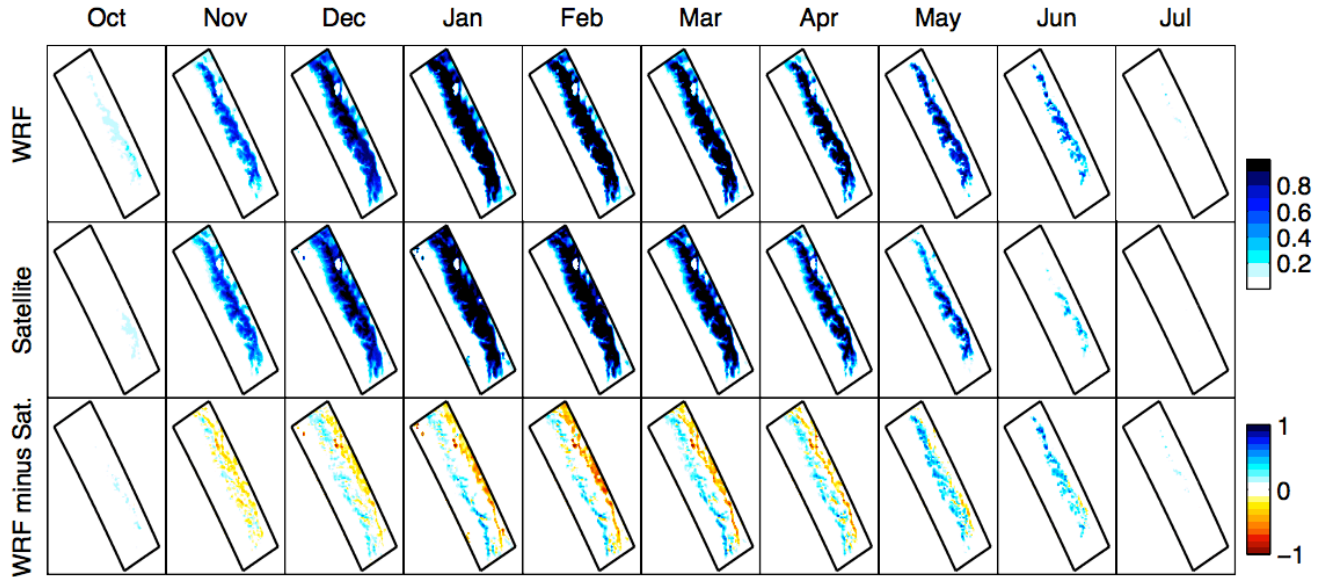


Figure 4: Monthly snow covered fraction climatology (April 2000–December 2006) for WRF resampled to the MODIS/Terra 0.05 degree grid (top row), MODIS/Terra (middle row), and WRF minus MODIS/Terra (bottom row).

Because snow albedo feedback ends up being such an important factor shaping Sierra Nevada warming patterns, we evaluate WRF’s simulation of snow cover. We define snow cover (abbreviated SCF) as the fraction of a grid cell covered by snow. For comparison, we use satellite data from MODIS/Terra Snow Cover Monthly L3 Global 0.05-Degree CMG Version 5 (Hall et al. 2006). MODIS/Terra Coverage begins in April 2000, providing some overlap with the baseline WRF simulation (which extends from 1981–2006). We compare monthly composite MODIS/Terra and WRF SCF patterns for April 2000 – December 2006 (Figure 4). WRF is linearly interpolated from 3-km resolution to 0.05-degree resolution to match MODIS/Terra. Overall, the patterns resemble one another closely, though a similar bias emerges in each month: WRF tends to produce slightly higher SCF than MODIS/Terra along the windward side of the Sierra Nevada and slightly lower SCF on the leeward side. Similar windward and leeward biases have occurred in previous WRF simulations (Wrzesien et al. 2014) and were attributed to underlying precipitation biases (Caldwell et al., 2009, Rögnvaldsson et al., 2011). In our simulation, these biases largely offset over the domain and total snow covered area (SCA; Figure 5) is similar. The high correlation of the monthly totals ($r = 0.94$) combined with their positioning along the line $y = x$ (red) indicates that WRF simulates the seasonal cycle and interannual variability of SCA with a high degree of accuracy. One exception is that WRF tends to overestimate SCA relative to MODIS/Terra in October and June—months at the beginning and end of the snow season with little snow. Generally, WRF captures the observed effects of temperature variability on snow cover over the course of the seasonal cycle, which provides some evidence that WRF will also be able to realistically capture the most important effects of large-scale and sustained temperature anomalies on snow cover in the future climate simulations performed here. In other words, WRF simulates SCF with some degree of accuracy. Although WRF is not perfect, it is most likely realistic enough to capture the major features of the climate change signals in the region, including the effect of snow albedo feedback.

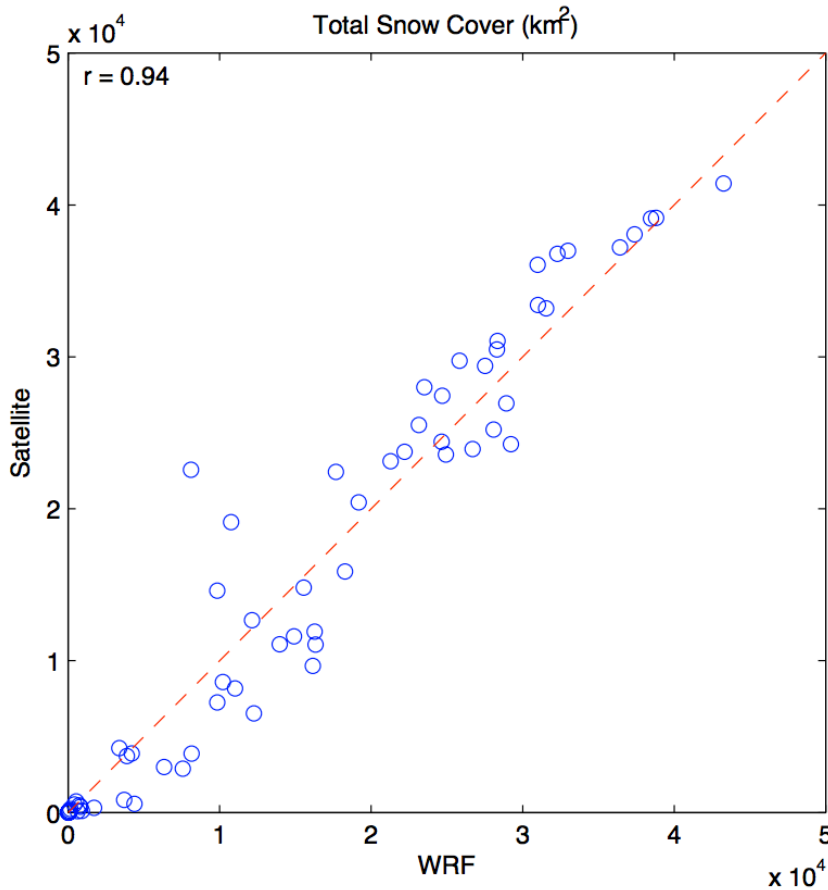


Figure 5: Monthly snow covered area (km^2) in the innermost domain for the period April 2000 – December 2006 for the MODIS/Terra satellite versus WRF (blue circles). The line $y = x$ is drawn for reference (red). A Pearson correlation coefficient of 0.94 was calculated excluding months where both the WRF and satellite show virtually no snow (defined as total snow cover less than $0.2 \cdot 10^4 \text{ km}^2$).

WRF climate changes

Downscaled climate changes are calculated by differencing the climates of the five future simulations and the climate of the 1991–2000 sub-period of the historical simulation. Note that these changes represent a downscaling of the differences in global climate model climate between the 2081–2100 and 1981–2000 periods. The dynamically downscaled warming patterns are compared to those produced by two commonly used statistical downscaling methods: Bias Correction and Constructed Analogs (BCCA; Hidalgo et al. 2008; Maurer and Hidalgo 2008) and Bias Correction with Spatial Disaggregation (BCSD; Wood et al. 2002; Wood et al. 2004; Maurer 2007). The BCCA and BCSD projections presented here were obtained online from the archive of Downscaled CMIP3 and CMIP5 Climate and Hydrology Projections (Reclamation 2013). BCCA projections are available for daily maximum (Tmax) and minimum (Tmin) with native resolution of $1/8^{\text{th}}$ degree, which are averaged together to produce monthly average temperatures and linearly interpolated to the 3 km WRF grid. Similar processing was applied to BCSD Tmax and Tmin data (which are available as monthly averages). Linear interpolation is also included as the simplest and most naïve possible method for downscaling global climate model output, representing a standard measure of minimal downscaling skill against which the other methods can be compared.

All downscaling methods produce climate change patterns exhibiting reduced warming closer to the coast and higher warming inland of the Sierra Nevada (Figure 6). This gradient is a common large-scale feature of global climate model warming patterns. It arises from the contrast in warming over the continental inland interior and coastal areas subject to marine influence (Manabe et al. 1991; Cubasch et al. 2001; Braganza et al. 2003, 2004; Sutton et al. 2007; Joshi et al. 2008; Dong et al. 2009; Fasullo et al. 2010).

However, dynamical downscaling produces a sharper gradient than the other methods. We hypothesize that the high-resolution WRF configuration we use resolves the narrow width and high peaks of the Sierra Nevada, which act as a barrier preventing mixing of marine and high desert air masses and their accompanying properties. This effect is most apparent in the summer months, when the global climate models' land-sea contrast in warming is greatest.

Dynamical downscaling also exhibits significant warming amplification due to snow albedo feedback. Locations with baseline temperatures near the freezing point are vulnerable to snow cover loss in a warmer climate due to less snowfall as a fraction of precipitation (S/P) and earlier snowmelt. From December through April, only the lower and middle elevations (~1000–3000 m) are vulnerable to snow cover loss and enhanced warming, while high elevations (> 3000 m) are relatively unaffected (Figure 6, bottom row). At the beginning of the snow season (October–November) and the end (May–July), baseline temperatures are high enough that snow cover at all elevations is vulnerable to loss. The strength of snow albedo feedback is greatest in the spring and early summer, when higher insolation levels cause the same albedo reduction to result in more absorbed solar radiation at the surface. The strength of the feedback also varies spatially in some months. From November to May, higher insolation in the eastern and southern Sierra Nevada causes the warming enhancement per SCF change to be equal or larger than in the northern and western Sierra Nevada.

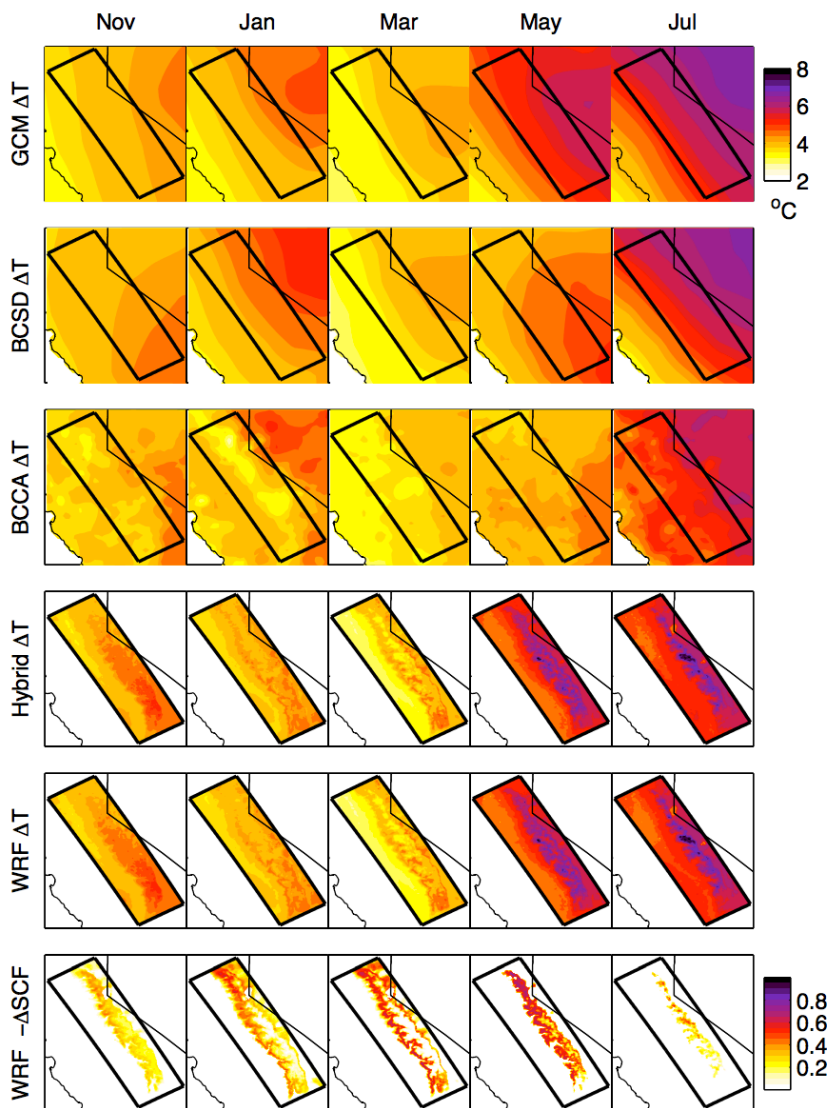


Figure 6: Changes in selected monthly temperature climatologies averaged over five GCMs downscaled multiple ways: (first row) linear interpolation, (second row) BCSD, (third row) BCCA, (fourth row) the hybrid statistical model, (fifth row) WRF. Decreases in WRF SCF are also shown (bottom row). The innermost WRF domain is outlined in black.

Snow albedo feedback is a critical feature of the warming’s elevational profile for many months (Figure 7). The linearly interpolated global climate model warming (red lines), BCSD-downscaled warming (magenta lines), and BCCA-downscaled warming (green lines) all mostly lack this elevation-dependent signal evident in WRF (black lines). It is not surprising that global climate models do not have high enough resolution to capture the snow-albedo feedback enhancement of the warming in the Sierra Nevada. However, when interpolated, the global climate models do show a smoothly varying contrast between the low-elevation Central Valley and the mid-elevation interior on the leeward side of the Sierra Nevada (visible in Figure 7 top row), which leads to an apparent elevational gradient (Figure 7, red lines). This gradient is relatively weak, restricted to below about 2000 m, and the snow albedo feedback enhancement band is missed entirely. BCSD produces very similar patterns to the interpolated global climate model warming (Figure 6 second row). In fact, BCSD warming patterns are, by construction, those of the interpolated bias-corrected global climate model, and therefore have similar shortcomings. BCCA should, in theory, better capture the elevational gradients in the warming, given that it uses relatively high-resolution ($1/8^{\text{th}}$ degree) historical analogs. These analogs could conceivably capture spatial variations leading to the elevational gradients. However, warming patterns produced by BCCA show no apparent effects of snow-albedo feedback (Figure 6, third row). BCCA produces weaker elevational gradients than the interpolated global climate model patterns and consistently produces less warming than the others at nearly all elevations in our domain (Figure 7, green lines). We argue that snow albedo feedback is a key process shaping warming patterns in the Sierra Nevada, and therefore the warming patterns produced by these statistical downscaling techniques lack a vital element of physical realism. This motivated us to develop a hybrid dynamical-statistical downscaling method that could capture such important features (Figure 7, blue lines).

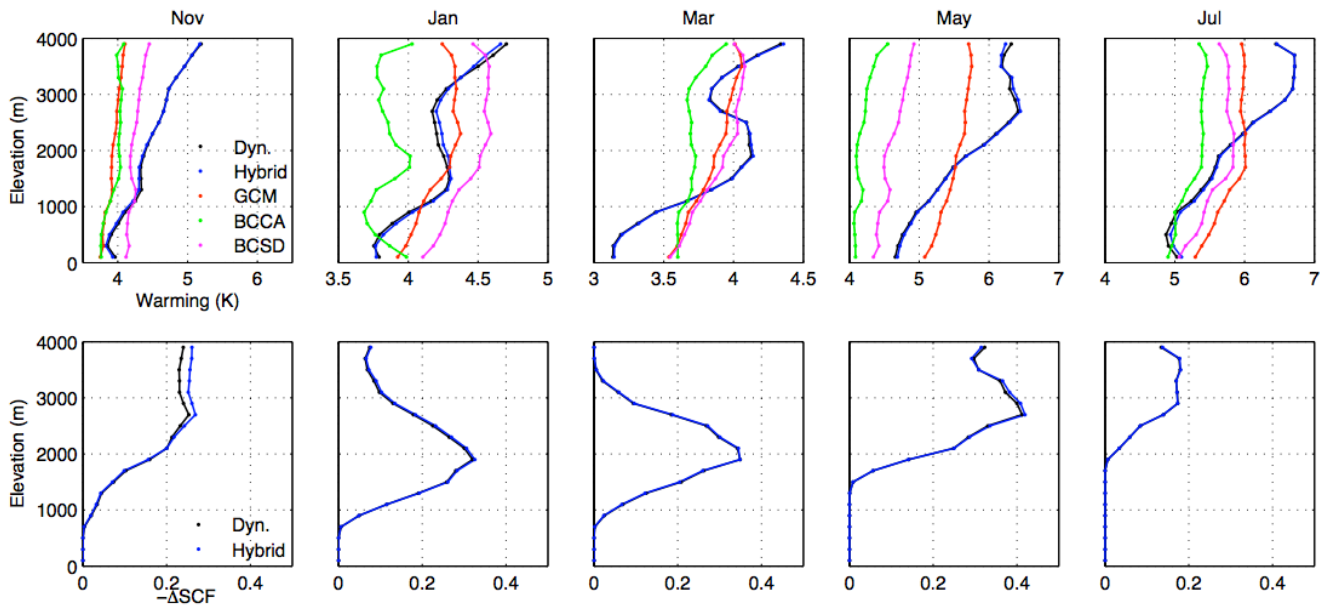


Figure 7: Comparison of monthly-mean elevational profiles of warming (top) and SCF loss (bottom) averaged over the five dynamically downscaled GCMs. The warming signal is downscaled using five methods: dynamical downscaling with WRF (black), hybrid downscaling (blue), interpolation of the GCM warming pattern (red), BCCA (green), and BCSD (magenta). Snow cover changes can only be generated with dynamical and hybrid statistical downscaling. The patterns produced by each downscaling method are interpolated to the WRF grid and then binned by elevation using WRF elevation. A bin size of 200 meters is used.

Discussion

The results of this study should be viewed with the following caveats in mind. First, results depend on the ability of WRF and the land surface model Noah-MP to realistically simulate snow albedo feedback. WRF simulates slightly more baseline snow cover than the MODIS/Terra satellite along the western slopes of the Sierra Nevada and less on the eastern slopes (Figure 4). Therefore, actual losses in absolute

snow cover and the resulting warming enhancements are likely to be smaller along the western slopes and larger on the eastern slopes than projected here. In June and July, WRF simulates a historical climatology of snow cover that is systematically higher than that shown by MODIS/Terra. So, actual snow cover losses and the resulting warming enhancements for June and July are likely to be smaller than those projected by WRF. Other factors also influence the strength of snow albedo feedback. The vegetation masking effect and treatment of snow albedo processes have been shown to affect snow albedo feedback (Qu and Hall 2007). Future work could explore the sensitivity of snow albedo feedback strength to key parameters in the land surface model.

Acknowledgements

Primary funding for this work was provided by the Metabolic Studio in partnership with the Annenberg Foundation (Grant #12-469: "Climate Change Projections in the Sierra Nevada"). Additional support was provided by the National Science Foundation (Grant #EF-1065853, "Collaborative Research: Do Microenvironments Govern Macroecology?"). The authors are not aware of any conflicts of interest.

PRISM data is available from <http://www.prism.oregonstate.edu/> (Daly et al. 2008). MODIS/Terra snow cover data is available from <http://nsidc.org/data/MOD10CM> (Hall et al. 2006). CMIP5 BCCA and BCSD data can be found at http://gdo-dcp.ucllnl.org/downscaled_cmip_projections/ (Reclamation 2013).

For more information

For more information about the UCLA dynamically downscaled data set, contact Prof. Alex Hall at alexhall@atmos.ucla.edu.

Table 1. Details of the 5 CMIP5 global climate models dynamically downscaled. For a particular global climate model, averages were taken over all available realizations in order to damp out internal variability. Realizations used for each global climate model are noted in the rightmost column.

Model	Country	Institute	Realization(s)
CNRM-CM5	France	Centre National de Recherches Meteorologiques	r1i1p1, r2i1p1, r4i1p1, r6i1p1
GFDL-CM3	USA	NOAA Geophysical Fluid Dynamics Laboratory	r1i1p1
inmcm4	Russia	Institute for Numerical Mathematics	r1i1p1
IPSL-CM5A-LR	France	Institut Pierre Simon Laplace	r1i1p1, r2i1p1, r3i1p1, r4i1p1
MPI-ESM-LR	Germany	Max Planck Institute for Meteorology	r1i1p1, r2i1p1, r3i1p1

References

- Benestad, R. E., I. Hanssen-Bauer, and D., Chen, 2008: *Empirical-statistical Downscaling*. World Scientific, 228pp.
- Berg, N., A. Hall, F. Sun, S. Capps, D. Walton, B. Langenbrunner, and D. Neelin, 2015: Twenty-First-Century Precipitation Changes over the Los Angeles Region. *J. Climate.*, **28**, 401–421, doi:10.1175/JCLI-D-14-00316.1.
- Braganza, K., D. J. Karoly, A. C. Hirst, M. E. Mann, P. Stott, R. J. Stouffer, and S. F. B. Tett, 2003: Simple indices of global climate variability and change: Part I—Variability and correlation structure. *Climate Dyn.*, **20**, 491–502, doi:10.007/s00382-002-0286-0.
- Caldwell, P. M., H.-N. S. Chin, D. C. Bader, and G. Bala, 2009: Evaluation of a WRF based dynamical downscaling simulation over California. *Climatic Change*, **95**, 499–521, doi:10.1007/s10584-009-9583-5.
- Cubasch, U., and Coauthors, 2001: Projections of future climate change. *Climate Change 2001: The Scientific Basis*. J. T. Houghton et al., Eds., Cambridge University Press, 525–582.
- Daly, C., and Coauthors, 2008: Physiographically-sensitive mapping of temperature and precipitation across the conterminous United States. *Int. J. Climatology.*, **28**, 2031–2064, doi:10.1002/joc.1688.
- Dayon G., J. Boé, and E. Martin, 2015: Transferability in the future climate of a statistical downscaling method for precipitation in France. *J. Geophys. Res. Atmos.*, **120**, 1023–1043, doi: 10.1002/2014JD022236.
- Dixon, K. W., J. R. Lanzante, M. J. Nath, K. Hayhoe, A. Stoner, A. Radhakrishnan, V. Balaji, C. F. Gaitán, 2016: Evaluating the stationarity assumption in statistically downscaled climate projections: is past performance an indicator of future results? *Climatic Change*, available online, 1-14, doi:10.1007/s10584-016-1598-0.
- Dong, B., J. M. Gregory, and R. T. Sutton, 2009: Understanding land-sea warming contrast in response to increasing greenhouse gases, Part I: transient adjustment. *J. Climate*, **22**, 3079–3097, doi:10.1175/2009JCLI2652.1.
- Dudhia, J., 1989: Numerical study of convection observed during the winter monsoon experiment using a mesoscale two-dimensional model. *J. Atmos. Sci.*, **46**, 3077–3107, doi:10.1175/1520-0469(1989)046<3077:NSOCOD>2.0.CO;2.
- Fasullo, J. T., 2010: Robust land–ocean contrasts in energy and water cycle feedbacks. *J. Climate*, **23**, 4677–4693, doi:10.1175/2010JCLI3451.1.
- Giorgi, F., J. W. Hurrell, M. R. Marinucci, and M. Beniston, 1997: Elevation dependency of the surface climate change signal: A model study. *J. Climate*, **10**, 288–296. doi:10.1175/1520-0442(1997)010<0288:EDOTSC>2.0.CO;2.
- Giorgi, F., and Coauthors, 2001: Regional climate information—evaluation and projections. *Climate Change 2001: The Scientific Basis*. J. T. Houghton et al., Eds., Cambridge University Press, 583–638.
- Guilyardi, E., and Coauthors, 2009: Understanding El Niño in Ocean–Atmosphere General Circulation Models: Progress and Challenges. *Bull. Amer. Meteor. Soc.*, **90**, 325–340, doi:10.1175/2008BAMS2387.1.
- Gutiérrez, J. M., D. San-Martín, S. Brands, R. Manzananas, and S. Herrera, 2013: Reassessing Statistical Downscaling Techniques for Their Robust Application under Climate Change Conditions. *J. Climate*, **26**, 171–188, doi:10.1175/JCLI-D-11-00687.1.
- Hall, D. K., V. V. Salomonson, and G. A. Riggs, 2006: MODIS/Terra Snow Cover Monthly L3 Global 0.05 Deg CMG, Version 5. April 2000 – December 2006 subset. Boulder, Colorado USA. NSIDC:

National Snow and Ice Data Center. Accessed 31 July 2015. [Available online at <http://dx.doi.org/10.5067/IPPLURB6RPCN>]

- Hidalgo, H. G., M. D. Dettinger, D. R. Cayan, 2008: Downscaling with constructed analogues: daily precipitation and temperature fields over the United States. California Energy Commission technical report CEC-500-2007-123, 48 pp.
- Joshi, M. M., J. M. Gregory, M. J. Webb, D. M. Sexton, and T. C. Johns, 2008: Mechanisms for the land/sea warming contrast exhibited by simulations of climate change. *Climate Dyn.*, **30**, 455–465, doi:10.1007/s00382-007-0306-1.
- Kain, J. S., and J. M. Fritsch, 1990: A one-dimensional entraining/detraining plume model and its application in convective parameterization. *J. Atm. Sci.*, **47**(23), 2784–2802, doi:10.1175/1520-0469(1990)047<2784:AODEPM>2.0.CO;2.
- Kapnick, S., and A. Hall, 2010: Observed Climate–Snowpack Relationships in California and their Implications for the Future. *J. Climate*, **23**, 3446–3456, doi:10.1175/2010JCLI2903.1
- Kawase, H., T. Yoshikane, M. Hara, F. Kimura, T. Yasunari, B. Ailikun, H. Ueda, and T. Inoue, 2009: Intermodel variability of future changes in the Baiu rainband estimated by the pseudo global warming downscaling method. *J. Geophys. Res.*, **114**, D24110, doi:10.1029/2009JD011803.
- Kim, J., 2001: A nested modeling study of elevation-dependent climate change signals in California induced by increased atmospheric CO₂. *Geophys. Res. Lett.*, **28**, 2951–2954, doi:10.1029/2001GL013198.
- Letcher, T. W., J. R. Minder, 2015: Characterization of the simulated regional snow albedo feedback using a regional climate model over complex terrain. *J. Climate*, **28** (19), 7576–7595, doi:10.1175/JCLI-D-15-0166.1.
- Manabe, S., R. J. Stouffer, M. J. Spelman, and K. Bryan, 1991: Transient responses of a coupled ocean-atmosphere model to gradual changes of atmospheric CO₂. Part I. Annual mean response. *J. Climate*, **4**(8), 785–818, doi:10.1175/1520-0442(1991)004<0785:TROACO>2.0.CO;2.
- Maraun, D., and Coauthors, 2010: Precipitation downscaling under climate change: Recent developments to bridge the gap between dynamical models and the end use. *Rev. Geophys.*, **48**, RG3003, doi:10.1029/2009RG000314.
- Maurer, E. P., 2007: Uncertainty in hydrologic impacts of climate change in the Sierra Nevada, California, under two emissions scenarios. *Climatic Change*, **82**, 309–325, doi:10.1007/s10584-006-9180-9.
- Maurer, E. P., and H. G. Hidalgo, 2008: Utility of daily vs. monthly large-scale climate data: an intercomparison of two statistical downscaling methods. *Hydrol. Earth Syst. Sci.*, **12**, 551–563, doi:10.5194/hess-12-551-2008.
- Mesinger, F., and Coauthors, 2006: North American regional reanalysis. *Bull. Amer. Meteor. Soc.*, **87**(3), 343–360, doi:10.1175/BAMS-87-3-343.
- Mlawer, E. J., S. J., Taubman, P. D. Brown, M. J. Iacono, and S. A. Clough, 1997: Radiative transfer for inhomogeneous atmospheres: RRTM, a validated correlated-k model for the longwave, *J. Geophys. Res.*, **102**(D14), 16663–16682, doi:10.1029/97JD00237.
- Nakanishi, M., and H. Niino, 2006: An improved Mellor-Yamada Level-3 model: Its numerical stability and application to a regional prediction of advection fog. *Boundary-Layer Meteor.*, **119**, 397–407, doi:10.1007/s10546-005-9030-8.
- Niu, G.-Y., and Coauthors, 2011: The community Noah land surface model with multiparameterization options (Noah-MP): 1. Model description and evaluation with local-scale measurements. *J. Geophys. Res.*, **116**(D12109), doi:10.1029/2010JD015139.

- Pierce, D. W., and D. R. Cayan, 2013a: The Uneven Response of Different Snow Measures to Human-Induced Climate Warming. *J. Climate*, **26**, 4148–4167. doi: 10.1175/JCLI-D-12-00534.1.
- Pierce, D.W., and Coauthors, 2013b: Probabilistic estimates of future changes in California temperature and precipitation using statistical and dynamical downscaling. *Climate Dyn.*, **40**(3-4), 839–856, doi:10.1007/s00382-012-1337-9.
- Pepin, N., and Coauthors, 2015: Elevation-dependent warming in mountain regions of the world. *Nature Climate Change*, **5**(5), 424. doi:10.1038/nclimate2563.
- Qu, X., and A. Hall., 2007: What controls the strength of snow albedo feedback? *J. Climate*, **20**, 3971–3981. doi: 10.1175/JCLI4186.1
- Qu, X., and A. Hall, 2014: On the persistent spread of snow-albedo feedback. *Climate Dyn.*, **42**(1–2), 69–81, doi:10.1007/s00382-013-1945-z.
- Rasmussen, R., C. Liu, K. Ikeda, D. Gochis, D. Yates, F. Chen, and E. Gutmann, 2011: High-resolution coupled climate runoff simulations of seasonal snowfall over Colorado: A process study of current and warmer climate. *J. Climate*, **24**(12), 3015–3048, doi:10.1175/2010JCLI3985.1.
- Rangwala, I., and J. R. Miller, 2012: Climate change in mountains: a review of elevation- dependent warming and its possible causes. *Climatic Change*, **114**, 527–547, doi:10.1007/s10584-012-0419-3.
- Reclamation, 2013: Downscaled CMIP3 and CMIP5 Climate and Hydrology Projections: Release of Downscaled CMIP5 Climate Projections, Comparison with preceding Information, and Summary of User Needs. Prepared by the U.S. Department of the Interior, Bureau of Reclamation, Technical Services Center, Denver, Colorado. 47 pp.
- Rögnvaldsson, Ó., J. W. Bao, H. Ágústsson, and H. Ólafsson, 2011: Downslope windstorm in Iceland – WRF/MM5 model comparison. *Atmos. Chem. Phys.*, **11**, 103–120, doi:10.5194/acp-11-103-2011.
- Sato T., F. Kimura, and A. Kitoh, 2007: Projection of global warming onto regional precipitation over Mongolia using a regional climate model. *J. Hydrology*, **333**, 144–154, doi:10.1016/j.jhydrol.2006.07.023.
- Schär, C., C. Frie, D. Lüthi, and H. C. Davies, 1996: Surrogate climate-change scenarios for regional climate models. *Geophys. Res. Lett.*, **23**, 669–672.
- Skamarock, W. C., and Coauthors, 2008: A description of the Advanced Research WRF version 3. *NCAR Technical Note*, NCAR/TN-4751+STR.
- Sun F., D. B. Walton, A. Hall, 2015: A Hybrid Dynamical–Statistical Downscaling Technique. Part II: End-of-Century Warming Projections Predict a New Climate State in the Los Angeles Region. *J. Climate*, **28**(12), 4618–4636, doi:10.1175/JCLI-D-14-00197.1.
- Sutton, R. T., B. Dong, and J. M. Gregory, 2007: Land/sea warming ratio in response to climate change: IPCC AR4 model results and comparison with observations. *Geophys. Res. Lett.*, **34**(2), L02701, doi: 10.1029/2006GL028164.
- Taylor, K. E., R. J. Stouffer, and G. A. Meehl, 2012: An overview of CMIP5 and the experiment design. *Bull. Amer. Meteor. Soc.*, **93**(4), 485–498, doi:10.1175/BAMS-D-11-00094.1.
- Tebaldi, C., R. L. Smith, D. Nychka, and L. O. Mearns, 2005: Quantifying uncertainty in projections of regional climate change: A Bayesian approach to the analysis of multimodel ensembles. *J. Climate*, **18**(10), 1524–1540, doi:10.1175/JCLI3363.1.
- Thompson, G., P. R. Field, R. M. Rasmussen, and W. D. Hall, 2008: Explicit Forecasts of Winter Precipitation Using an Improved Bulk Microphysics Scheme. Part II: Implementation of a New Snow Parameterization. *Mon. Wea. Rev.*, **136**, 5095–5115, doi:10.1175/2008MWR2387.1.

- Walton, D. B., S. Fengpeng, A. Hall, and S. Capps, 2015: A Hybrid Dynamical–Statistical Downscaling Technique. Part I: Development and Validation of the Technique. *J. Climate*, **28**(12), 4597–4617, doi:10.1175/JCLI-D-14-00196.1.
- Walton DB, A Hall, N Berg, M Schwartz, and F Sun, 2016: Downscaled CMIP5 projections of elevation dependent warming and snow cover loss in California's Sierra Nevada. *Journal of Climate*, submitted.
- Wilby, R. L., and T. M. L. Wigley, 1997: Downscaling general circulation model output: a review of methods and limitations. *Prog. Phy. Geog.*, **21**(4), 530–548, doi:10.1177/030913339702100403.
- Wood, A. W., E. P. Maurer, A. Kumar, and D. P. Lettenmaier, 2002: Long-range experimental hydrologic forecasting for the eastern United States. *J. Geophys. Res.*, **107**(D20), 4429, doi:10.1029/2001JD000659.
- Wood, A. W., L. R. Leung, V. Sridhar, and D. P. Lettenmaier, 2004: Hydrologic implications of dynamical and statistical approaches to downscaling climate model outputs. *Climatic Change*, **62**,189–216, doi:10.1023/B:CLIM.0000013685.99609.9e.
- Wrzesien, M. L., T. M. Pavelsky, S. B. Kapnick, M. T. Durand, and T. H. Painter, 2014: Evaluation of snow cover fraction for regional climate simulations in the Sierra Nevada. *Int. J. Climatol.*, **35**, 2472–2484, doi:10.1002/joc.4136.